Theory of magnetic-field-dependent alloy broadening of exciton-photoluminescence linewidths in semiconductor alloys

S. K. Lyo
Sandia National Laboratories, Albuquerque, New Mexico 87185
(Received 17 February 1993)

A theory is developed for the inhomogeneous photoluminescence line shape and, in particular, the linewidth of excitons due to alloy disorder in undoped semiconductor alloys in the presence of external magnetic fields. In contrast to previous theories, we find that both the linewidth and its field dependence depend not only on the exciton wave function for the electron-hole relative motion but also depend sensitively on the localization length R_0 of the center-of-mass wave function. In general, the line shape depends on the nature of the exciton localization. The linewidths arise from the fluctuations of the conduction- and valence-band edges in the localization region where there is significant amplitude of the total exciton wave function. The wave function for the relative motion is calculated numerically by reducing the Schrödinger equation to a difference equation at arbitrary fields, while the center-of-mass wave function is treated phenomenologically. The linewidth is calculated as a function of the magnetic field and the localization length R_0. The results yield good agreement with recent experimental data from $In_{0.48}Ga_{0.52}P$.

I. INTRODUCTION

Semiconductor alloys have received increasing attention recently because their band gaps and lattice constants can be tailored for useful applications in optoelectronic and photonic devices. The low-temperature photoluminescence line shape reveals important information about the effective band gap, the homogeneity of the sample, and possible order-disorder phase transitions. When the laser power is low, photogenerated excitons in a disordered system relax quickly to the band-tail states and become localized. These low-energy excitons localize in different regions of the sample and luminesce at different photon energies due to spatially varying local conduction- and valence-band edges caused by the random alloy composition. As a result, inhomogeneous photoluminescence linewidths yield information about the alloy-energy fluctuations occurring within the length scale of the exciton wave function. In addition, they provide information about possible domain-energy fluctuations, if present, over a much larger length scale. Magnetic fields are expected to affect mainly the size of the exciton wave function and therefore yield additional information about the former contribution.

Several authors have studied alloy broadening experimentally[1,2] and theoretically.[1–5] The basic physics behind alloy broadening is as follows.[1–3] The alloy composition inside the volume occupied by one exciton is different from that inside the volume of another exciton; this yields an inhomogeneously broadened exciton energy and thus an inhomogeneous photoluminescence linewidth. The linewidth was obtained from the root-mean-square deviation of the local band-gap fluctuation inside the volume Ω_{ex} of an exciton. The exciton volume was equated to $\Omega_{ex}=4\pi/3\langle r^3\rangle$ where the expectation value (designated by the angular brackets) is taken with respect to the wave function $\psi(\mathbf{r})$ of the electron-hole relative coordinate $\mathbf{r}=\mathbf{r}_e-\mathbf{r}_h$ (i.e., the hydrogenic wave function).[1] The linewidth is then inversely proportional to the square root of the number of the sites inside Ω_{ex} and therefore proportional to $\Omega_{ex}^{-1/2}$. Realizing that such a definition of the exciton volume is somewhat arbitrary, Lee and Bajaj[4] (LB) made significant progress toward a microscopic approach by expressing the linewidth in terms of the exciton wave function rather than the volume Ω_{ex}. They introduced a spatially dependent random local band-gap fluctuation $E_g(\mathbf{r})$ and took an expectation value of $E_g(\mathbf{r})$ with respect to the wave function $\psi(\mathbf{r})$ for the local deviation of the exciton energy from the mean value. As a result, the linewidth was shown to be proportional to the square root of the expression $\int\psi(\mathbf{r})^4 d^3r$. An interesting idea of controlling the linewidth by applying an external magnetic field was also pioneered by Bajaj's group,[5] who proposed that the field shrinks the exciton volume and therefore increases the linewidth. A field-dependent linewidth (which increases approximately from 4.5 meV to 6 meV as the field increases from zero to 13.6 T) was recently observed from disordered $In_{0.48}Ga_{0.52}P$ by Jones *et al.*[6]

The theoretical treatments described above, however, have two serious limitations. First, only the electron-hole relative motion [e.g., Ω_{ex} and $\psi(\mathbf{r})$] was explicitly considered. Second, the local exciton energy was determined entirely by the local random band-gap energy fluctuation $E_g(\mathbf{r})$. As will be discussed qualitatively below and more completely in the later sections, these approximations or assumptions can lead to qualitatively incorrect results. In a disordered medium, the resonant photon energy from an exciton is determined not by the relative coordinate but by the absolute positions of the electron and the hole. Therefore, it is necessary to treat the electron and hole coordinates independently from the beginning. Be-

0163-1829/93/48(4)/2152(10)/$06.00

cause the electron and the hole are not at the same position most of the time, the basic random parameter in our treatment is the nonlocal band-gap energy fluctuation $E_g(\mathbf{r}_e,\mathbf{r}_h)=E_e(\mathbf{r}_e)+E_h(\mathbf{r}_h)$ which is the sum of the separate local band-edge fluctuations of the electron $[E_e(\mathbf{r}_e)]$ and the hole $[E_h(\mathbf{r}_h)]$ rather than $E_g(\mathbf{r})$. In our approach, the total exciton wave function $\Psi(\mathbf{r}_e,\mathbf{r}_h)=\Phi(\mathbf{R})\psi(\mathbf{r})$ is a product of the wave functions of the center-of-mass coordinate ($\mathbf{R}$) and the relative coordinate ($\mathbf{r}$). The center-of-mass wave function $\Phi(\mathbf{R})$ describes where and how the center of mass of the exciton is localized and is insensitive to the magnetic field, while the relative wave function $\psi(\mathbf{r})$ is field dependent. The true exciton volume $\tilde{\Omega}_{\rm ex}$ is then determined not only by $\psi(\mathbf{r})$ but also by $\Phi(\mathbf{R})$.

The role of the function $\Phi(\mathbf{R})$ is clearly seen in the following extreme limits. If the exciton is in a free motion [i.e., $\Phi(\mathbf{R})$ is a plane wave] or is localized in an infinitely large volume, the fluctuation inside $\tilde{\Omega}_{\rm ex}$ becomes zero, yielding a vanishing linewidth. Therefore, a large inhomogeneous linewidth is expected only from a reasonably small localization radius (R_0) of the center of mass. In the opposite limit of sharp pinning of the exciton (i.e., R_0 is of the order of the lattice constant), we recover the results of LB,[4] only if the valence-band-edge fluctuation [i.e., $E_h(r_h)$] is zero.

In general, the inhomogeneous linewidth has two sources of contributions, namely (1) the field-independent part which arises from the alloy fluctuation seen by the center of mass and (2) the field-dependent part which originates from the alloy fluctuation inside the region where $|\psi(\mathbf{r})|^2$ is significant. The latter contribution decreases with increasing R_0. It is then essential to look for the source and the nature of the exciton localization in order to explain field-dependent linewidths observed in the group III-V (or II-VI) semiconductor alloys, as exemplified by disordered $In_{0.48}Ga_{0.52}P$.

In this paper two possibilities of the exciton localization are examined, namely pinning by defect centers and localization by alloy disorder. We show that the inhomogeneous linewidth (and its field-dependence) is sensitive to the exciton center-of-mass localization length R_0 as well as to the exciton radius. The linewidth is found to depend significantly on the magnetic field only if the quantity R_0 is smaller than the exciton radius. If R_0 is large, the field-dependent as well as the field-independent linewidth arising from microscopic alloy disorder is small. However, there can be macroscopic inhomogeneity or domains of varying alloy compositions, yielding field-independent inhomogeneous linewidths. These results are consistent with recent data which show that only a small number of systems display field-dependent linewidths (corresponding to small R_0), while a large number of systems show broad field-independent linewidths.[7]

The main emphasis of this paper is the field-dependent linewidth arising from the exciton localization. In this case, the linewidth depends on the overlap integrals of powers of the center-of-mass and relative wave functions. The function $\psi(\mathbf{r})$ is calculated by employing a rigorous numerical method at arbitrary fields by converting the Schrödinger equation to a five-point difference equation in magnetic fields.[8] Our numerical approach is expected to yield more reliable results for $\psi(\mathbf{r})$ than a variational method,[5] because variational methods give more accurate results for the binding energy than for the wave function. The linewidth is calculated as a function of the magnetic field and R_0. The calculated linewidth and line shape yield reasonable agreement with recent magnetoluminescence data[6] from disordered $In_{0.48}Ga_{0.52}P$.

The paper is organized as follows. A formalism is developed for the inhomogeneous linewidth in Sec. II. A numerical evaluation of the exciton wave function and overlap parameters in magnetic fields is given in Sec. III. The linewidth and the line shape are studied as a function of the magnetic field in Sec. IV and compared with recent data.[6] Comparison of our results with those of LB (Ref. 4) is given. The paper is summarized in Sec. V.

II. FORMALISM

In this section we study two different models for the exciton localization. We first consider a simple case where excitons are localized by pinning centers. Second, we consider a more complicated case where the excitons are localized inside potential wells created by spatial fluctuations of the band-edge potentials introduced by the density fluctuation of the composite atoms such as In atoms in $In_xGa_{1-x}P$ alloys.

It is convenient to describe the motion of an electron and a hole interacting through a Coulomb potential in an external magnetic field B in terms of the relative ($\mathbf{r}$) and center-of-mass ($\mathbf{R}$) coordinates. The wave function for the relative coordinate satisfies[9]

$$H_{\rm r}\psi(\mathbf{r})=\epsilon_{\rm ex}(\mathbf{B})\psi(\mathbf{r}) , \tag{1}$$

where

$$H_{\rm r}=-\frac{\hbar^2}{2\mu}\nabla^2-\frac{e}{2c}\left[\frac{1}{m_e}-\frac{1}{m_h}\right]\mathbf{B}\cdot\mathbf{L}+\frac{e^2A^2}{2\mu c^2}-e^2/\kappa r . \tag{2}$$

Here $\nabla=\partial/\partial\mathbf{r}$, $\mathbf{L}=\mathbf{r}\times\mathbf{p}$, $\mathbf{p}=\hbar\nabla/i$, $\mathbf{A}=\frac{1}{2}\mathbf{B}\times\mathbf{r}$, and m_e,m_h,μ are the electron mass, hole mass, and the reduced mass, respectively. The quantities e, c, and $\hbar$ represent the electronic charge, speed of light, and Planck's constant divided by 2π. The dielectric constant κ is assumed to be uniform in the sample. The total envelope wave function Ψ of an exciton in a disordered alloy is given by[9]

$$\Psi(\mathbf{r}_e,\mathbf{r}_h)=\exp\left[-\frac{ie}{\hbar c}\mathbf{A}\cdot\mathbf{R}\right]\Phi(\mathbf{r}_e,\mathbf{r}_h)\psi(\mathbf{r}) , \tag{3}$$

and satisfies

$$H\Phi(\mathbf{r}_e,\mathbf{r}_h)\psi(\mathbf{r})=E\Phi(\mathbf{r}_e,\mathbf{r}_h)\psi(\mathbf{r}) , \tag{4}$$

where

$$H=H_{\rm r}+H_{\rm R}+H_{\rm rR}+V_e(\mathbf{r}_e)+V_h(\mathbf{r}_h) . \tag{5}$$

Here the first term was already defined in (2) and the second term describes the center-of-mass motion

$$H_{\mathbf{R}}=-\frac{\hbar^2}{2M}\nabla_{\mathbf{R}}^2+U(\mathbf{r}_e,\mathbf{r}_h)\ , \tag{6}$$

where $\nabla_{\mathbf{R}}=\partial/\partial\mathbf{R}$, $M=m_e+m_h$, and $U(\mathbf{r}_e,\mathbf{r}_h)$ denotes the potential energy of pinning centers, respectively. We assume that the separation between the pinning centers is much larger than the Bohr radius. The third term in (5) is defined as

$$H_{\mathbf{rR}}=\frac{2ie\hbar}{Mc}\mathbf{A}\cdot\nabla_{\mathbf{R}}\ . \tag{7}$$

The last two terms [i.e., $V_e(\mathbf{r}_e)$ and $V_h(\mathbf{r}_h)$] in (5) represent the random alloy fluctuations from the mean band-edge energies for the conduction and valence bands given by[4]

$$V_\alpha(\mathbf{r}_\alpha)=\sum_i E_\alpha(i)\Delta(\mathbf{r}_\alpha-\mathbf{R}_i),\quad \alpha=e,h\ , \tag{8a}$$

where the unit step function $\Delta(\mathbf{r}_\alpha-\mathbf{R}_i)$ equals unity inside a cell of volume ΔV around the lattice site $\mathbf{R}_i$ and vanishes outside this cell. The cell dimension is much smaller than the sizes of the wave functions Φ and ψ. The energy fluctuation $E_\alpha(i)$ (assumed to be positive above the bottom of the conduction band and below the top of the valence band) is random from cell to cell with a vanishing spatial average (i.e., $\langle E_\alpha\rangle=0$).

The alloy potential $V_\alpha(\mathbf{r}_\alpha)$ yields different local average energies for different excitons. For an exciton occupying a volume Ω_j, the local deviation of the band-edge energy from the sample-wide mean value is expected to be $E_j=(dE_\alpha/dx)(x_j-x)$, where x is the average concentration of, for example, In atoms (over the sample), x_j is the local concentration of In atoms inside Ω_j, and dE_α/dx is the first derivative of the band-edge energy for the conduction ($\alpha=c$) and valence ($\alpha=v$) bands with respect to the concentration x. The quantity E_j can be written as the sum of the band-edge fluctuation $E_\alpha(i)$ [defined in (8a)] over all the cells in Ω_j divided by the total number of the cells inside Ω_j. The quantity $E_\alpha(i)$ has an expression similar to that of E_j defined above except that $x_j=1$ ($x_j=0$) when the cell is occupied (vacant),

$$E_\alpha(i)=(1-x)(dE_\alpha/dx)\hat{\mathbf{n}}_i-x(dE_\alpha/dx)(1-\hat{\mathbf{n}}_i)\ , \tag{8b}$$

where $\hat{\mathbf{n}}_i=1,0$ is the occupation number of the ith cell, say, by an In atom.

A. Exciton localization due to pinning centers

An exciton can be localized by a pinning potential $U(\mathbf{r}_e,\mathbf{r}_h)$ due to defect centers, isoelectronic impurities, and acceptor or donor centers. The wave function $\Phi(\mathbf{r}_e,\mathbf{r}_h)$ depends on the nature of the pinning centers and in general is not known. However, it is sufficient for our purpose to characterize the wave function by the radius of localization R_0 and study how the quantity R_0 affects the exciton-photoluminescence linewidth. Thus, for the purpose of a numerical estimate, the center-of-mass ground-state exciton eigenfunction for (6) is assumed to be given by a Gaussian form

$$\Phi(\mathbf{R})=(\sqrt{\pi}R_0)^{-3/2}\exp(-R^2/2R_0^2)\ . \tag{9}$$

The last three terms in (5) [i.e., $H_{\mathbf{rR}}$, $V_e(\mathbf{r}_e)$, and $V_h(\mathbf{r}_h)$] are treated as a perturbation. In this approximation, the $H_{\mathbf{rR}}$ term in (7) does not contribute to the energy to the first order because of the parity but does yield a small second-order contribution. However, this term is independent of the disorder and thus does not contribute to the linewidth. Therefore, this term in (7) will be neglected.

The first-order correction for the alloy-fluctuation energy is given by the expectation value of the $V_e(\mathbf{r}_e)+V_h(\mathbf{r}_h)$ terms of (5) with respect to the ground state

$$\delta E=\sum_i\int\int[E_e(i)\Delta(\mathbf{r}_e-\mathbf{R}_i)+E_h(i)\Delta(\mathbf{r}_h-\mathbf{R}_i)]\times\rho(\mathbf{r})\zeta(\mathbf{R})d^3r\,d^3R\ , \tag{10}$$

where $\rho(\mathbf{r})=\psi(\mathbf{r})^2$ and $\zeta(\mathbf{R})=\Phi(\mathbf{R})^2$. Using $\langle E_\alpha(i)E_{\alpha'}(i')\rangle=\langle E_\alpha E_{\alpha'}\rangle\delta_{i,i'}$, where $\delta_{i,i'}$ is Kronecker's delta, the mean-square fluctuation is given from (10) by

$$\langle\delta E^2\rangle=\frac{\Delta V}{(2\pi)^3}\int\zeta_{\mathbf{k}}^2[\langle E_e^2\rangle\rho_{\mathbf{k}_h}^2+\langle E_h^2\rangle\rho_{\mathbf{k}_e}^2+2\langle E_eE_h\rangle\rho_{\mathbf{k}_h}\rho_{\mathbf{k}_e}]d^3k,\quad \mathbf{k}_h=\frac{m_h}{M}\mathbf{k},\quad \mathbf{k}_e=\frac{m_e}{M}\mathbf{k}\ . \tag{11}$$

Here the angular brackets denote the intracell average and the cell indices are dropped from $E_\alpha(i)$. The quantities

$$\rho_{\mathbf{k}}=\int\rho(\mathbf{r})\exp(i\mathbf{k}\cdot\mathbf{r})d^3r \tag{12a}$$

and

$$\zeta_{\mathbf{k}}=\int\zeta(\mathbf{r})\exp(i\mathbf{k}\cdot\mathbf{r})d^3r \tag{12b}$$

are dimensionless.

In the special case $m_e=m_h$, Eq. (11) becomes proportional to the gap fluctuation

$$\langle\delta E^2\rangle=\frac{\Delta V}{\pi^3}\langle(E_e+E_h)^2\rangle\int\zeta_{2\mathbf{k}}^2\rho_{\mathbf{k}}^2d^3k,\quad m_e=m_h\ .$$

In the limit of extreme localization (i.e., $\zeta_{2\mathbf{k}}=1$), this expression is similar to the result obtained by LB but with a very different coefficient.

To evaluate (11), we approximate $\rho_{\mathbf{k}_e}\approx1$ for the last term on the right-hand side of (11). This approximation is justified for $m_e\ll m_h$ because a significant contribution

to the integration arises only from the region $k_h a_B \leq 1$ where $\rho_{\mathbf{k}_h}$ is significantly large. In this region, however, we have $k_e a_B = (m_e/m_h) k_h a_B \ll 1$, and thus $\rho_{\mathbf{k}_e} \approx 1$. Here $a_B = \kappa\hbar^2/\mu e^2$ is the Bohr radius. Equation (11) is then rewritten without any other approximation as

$$\langle \delta E^2 \rangle = (\Delta V/a_B^3)[\eta_h^3 \langle E_e^2 \rangle \tilde{F}_{22}(\eta_h) + \eta_e^3 \langle E_h^2 \rangle \tilde{F}_{22}(\eta_e) + 2\eta_h^3 \langle E_e E_h \rangle \tilde{F}_{12}(\eta_h)] , \quad (13a)$$

which in the two limits of $R_0/a_B \gg m_e/M$ and $R_0/a_B \ll m_e/M$ reduces to

$$\langle \delta E^2 \rangle = (\Delta V/a_B^3)[\eta_h^3 \langle E_e^2 \rangle \tilde{F}_{22}(\eta_h) + \langle E_h^2 \rangle F_{02} + 2\eta_h^3 \langle E_e E_h \rangle \tilde{F}_{12}(\eta_h)] , \quad R_0/a_B \gg m_e/M \quad (13b)$$

and

$$\langle \delta E^2 \rangle = (\Delta V/a_B^3)[\{\eta_h^3 \langle E_e^2 \rangle + \eta_e^3 \langle E_h^2 \rangle\} F_{20} + 2\eta_h^3 \langle E_e E_h \rangle F_{10}], \quad R_0/a_B \ll m_e/M . \quad (13c)$$

Here $\eta_h = M/m_h$, $\eta_e = M/m_e$, and

$$\tilde{F}_{nm}(x) = (2\pi)^{-3} a_B^3 \int \rho_{\mathbf{k}}^n \zeta_{x\mathbf{k}}^m d^3k , \quad (14a)$$

and

$$F_{nm} = \tilde{F}_{nm}(1) = (2\pi)^{-3} a_B^3 \int \rho_{\mathbf{k}}^n \zeta_{\mathbf{k}}^m d^3k . \quad (14b)$$

In our model, $\zeta_{\mathbf{k}}$ is a function of kR_0 [cf. Eq. (9)]. Therefore $\tilde{F}_{nm}(x)$ can be obtained from F_{nm} by the replacement $R_0 \rightarrow xR_0$. It is then sufficient to study F_{nm} as a function of R_0 and the magnetic field.

The overlap parameters F_{nm} and $\tilde{F}_{nm}(x)$ represent the degree of overlap between the density functions $\rho(\mathbf{r})$ and $\zeta(\mathbf{R})$ in a real-coordinate representation. These overlap factors increase with the magnetic field for $n \neq 0$, because the field shrinks the exciton density function $\rho(\mathbf{r})$. In the limit $R_0/a_B \rightarrow 0$, one has $\zeta_k \rightarrow 1$ and thus

$$F_{12} \rightarrow F_{10} = a_B^3 \rho(0) \quad (15a)$$

and

$$F_{22} \rightarrow F_{20} = a_B^3 \int \rho(\mathbf{r})^2 d^3r . \quad (15b)$$

The second term of (13b) arises from the valence-band-edge fluctuation over the volume inside the center-of-mass wave function and equals $\langle E_h^2 \rangle \Delta V/[(2\pi)^{3/2} R_0^3]$ for the Gaussian wave function in (9). This contribution is independent of the magnetic field and can be significantly large for small R_0. Note that, apart from the special case $m_e = m_h$, the basic random quantities in (11) and (13) are the individual fluctuations of the conduction-band and valence-band edges $E_e(i)$ and $E_h(i')$, not the net gap fluctuation $E_g(i) = E_e(i) + E_h(i)$, in contradistinction with the results of LB. This result arises from the fact that the electron and hole are most of the time separated at different positions.

B. Exciton localization due to alloy disorder

We now examine the localization of excitons and its effect on the luminescence linewidth in the absence of pinning centers [i.e., $U(\mathbf{r}_e, \mathbf{r}_h) = 0$]. Localization of noninteracting electrons and holes through band-edge fluctuations introduced by the composition fluctuations in alloys has been studied previously in the absence of magnetic fields.[10,11] The following analysis is based on the treatment of Baranovski and Éfros (BE).[10] The density of the localized states are proportional to[10,11]

$$g(\epsilon) \propto (\epsilon/\epsilon_0)^{\nu} \exp(-\sqrt{\epsilon/\epsilon_0}) , \quad (16a)$$

where the energy $\epsilon > 0$ is measured from the mean band edge (i.e., mobility edge at $\epsilon = 0$) into the gap and[10]

$$\epsilon_0 = m_\alpha^3 x^2 (1-x)^2 (dE_\alpha/dx)^4 \Delta V^2/(178\hbar^6) . \quad (16b)$$

The exponent ν in (16a) equals $\nu = \frac{3}{2}$ for Gaussian potentials[11] employed for the present analysis. The localization radius is given by

$$R_0 \approx \hbar/(2m_\alpha \epsilon)^{1/2} . \quad (17)$$

The density of localized states $g(\epsilon)$ has a long tail, and as a result, a representative exciton energy ϵ is much larger than ϵ_0 except for the $\nu = 0$ case; the average energy and the root-mean-square deviation are given for $\nu = \frac{3}{2}$ by $\langle \epsilon \rangle = 30\epsilon_0$, and $\langle \delta\epsilon^2 \rangle^{1/2} = 27.9\epsilon_0$, while the full width at half maximum (FWHM) equals

$$\Delta\epsilon_{\mathrm{FWHM}} = 28.7\epsilon_0 . \quad (18a)$$

The FWHM is much smaller for $\nu = 0$ (considered by BE)

$$\Delta\epsilon_{\mathrm{FWHM}} = 0.48\epsilon_0 . \quad (18b)$$

The center-of-mass motion of an exciton becomes localized by fluctuating band-edge potentials. The Hamiltonian for the center-of-mass motion is thus found by taking the expectation value of (5) with respect to the wave function $\psi(\mathbf{r})$ for the relative motion. The net result is to absorb the last two terms of (5) into (6) by replacing the quantity $U(\mathbf{r}_e, \mathbf{r}_h)$ with their expectation values:

$$H_{\mathbf{R}} \Phi(\mathbf{R}) = (E - \epsilon_{\mathrm{ex}}) \Phi(\mathbf{R}) , \quad (19)$$

where

$$H_{\mathbf{R}} = -\frac{\hbar^2}{2M} \nabla_{\mathbf{R}}^2 + \tilde{V}_h(\mathbf{R}) + \tilde{V}_e(\mathbf{R}) , \quad (20)$$

$$\tilde{V}_e(\mathbf{R}) = \int V_e(\mathbf{r}_h + \mathbf{r}) \rho(\mathbf{r}) d^3r , \quad (21)$$

and

$$\tilde{V}_h(\mathbf{R}) = \int V_h(\mathbf{r}_h) \rho(\mathbf{r}) d^3r . \quad (22)$$

We approximate $\mathbf{r}_h \approx \mathbf{R}$ in (21) and (22) in the limit $m_e \ll m_h$, obtaining

$$\tilde{V}_h(\mathbf{R}) = V_h(\mathbf{R}) \quad (23a)$$

and

$$\tilde{V}_e(\mathbf{R}) = \int V_e(\mathbf{R} + \mathbf{r}) \rho(\mathbf{r}) d^3r . \quad (23b)$$

In the limit R_0 $[=\hbar/(2M\epsilon)^{1/2}] \gg a_B$, namely in the regime [$\epsilon_B = \mu e^4/(2\kappa^2\hbar^2)$ is the exciton binding energy]

$$\epsilon \ll \epsilon_c \equiv \frac{\mu}{M}\epsilon_B \ , \tag{24}$$

Eq. (23b) reduces to

$$\tilde{V}_e(\mathbf{R}) = V_e(\mathbf{R}) \ . \tag{23b'}$$

The last two terms in (20) then correspond to the band-gap (E_g) fluctuation, yielding for (16a) (Ref. 10)

$$\epsilon_0 = M^3 x^2 (1-x)^2 (dE_g/dx)^4 \Delta V^2/(178\hbar^6) \ . \tag{25}$$

In this case, the width of the exciton energy smearing is independent of the magnetic field. In $In_{0.48}Ga_{0.52}P/GaAs$, we use $m_h = 0.44$, $m_e = 0.091$, $\Delta V = a^4/4$, where $a = 5.66$ Å is the lattice constant, $dE_g/dx = 1.15$ eV,[13,14] obtaining $\epsilon_0 = 0.36$ meV.

On the other hand, in the regime R_0 $[=\hbar/(2M\epsilon)^{1/2}] \ll a_B$, namely for

$$\epsilon \gg \epsilon_c \ , \tag{26}$$

the quantity $\tilde{V}_e(R)$ becomes slowly varying in $\mathbf{R}$ because of the integration in $\mathbf{r}$ over a large volume $\propto a_B^3$ in (23b). In this case we can employ a mean-field approximation and replace $\tilde{V}_e(\mathbf{R})$ by its average with respect to $\zeta(\mathbf{R})$,

$$E = \epsilon_{\rm ex} + \epsilon_h + \int\int V_e(\mathbf{R}+\mathbf{r})\rho(\mathbf{r})\zeta(\mathbf{R}) d^3r \, d^3R \ , \tag{27}$$

where ϵ_h and $\Phi(\mathbf{R})$ [with $\zeta(\mathbf{R}) = \Phi(\mathbf{R})^2$] denote the eigenvalue and the eigenfunction of the first two terms in (20) (i.e., with only the valence-band-edge fluctuation present). The last term in (27) may also be interpreted as a first-order perturbation, since the r integration in (23b) makes $\tilde{V}_e(\mathbf{R})$ smaller than $V_e(\mathbf{R})$ because of the random cancellation effect. The density of states for ϵ_h in (27) is given by (16a) with

$$\epsilon_0 = M^3 x^2 (1-x)^2 (dE_v/dx)^4 \Delta V^2/(178\hbar^6) \ . \tag{28}$$

The last term in (27) is given by a Gaussian distribution with the mean-square deviation

$$\sigma^2 = \sigma_e^2 F_{22}, \quad \sigma_e^2 = (\Delta V/a_B^3)\langle E_e^2 \rangle \ , \tag{29}$$

where F_{22} is defined in (14).

Low-temperature luminescence data show no temperature dependence for the linewidth.[6] Therefore, we assume that the localized states are equally populated. The localization radius for $\zeta(\mathbf{R})$ in the expression of F_{22} in (29) is given by (17) with $m_\alpha = M$ and $\epsilon = \epsilon_h$. The quantity F_{22} depends on the magnetic field and, as will be shown later in Sec. III, is significantly large only in the limit of $R_0 \ll a_B$, namely when the most of the localized states lie in the region $\epsilon \gg \epsilon_c$. In this case, Eq. (29) reduces to

$$\sigma^2 = \sigma_e^2 F_{20} \ . \tag{30}$$

It is clear from the analysis in this section that the linewidth depends not only on the wave function of the electron-hole relative motion but also on the localization radius of the center-of-mass wave function: The linewidth vanishes, naturally, in the limit of a very large localization radius (i.e., $R_0 \gg a_B$), because the fluctuation in an infinitely large volume is zero.

III. EXCITON WAVE FUNCTION AND OVERLAP PARAMETERS

In this section we evaluate the exciton wave function and the overlap parameters F_{nm} and $\tilde{F}_{nm}(x)$ as a function of the magnetic field. The basic ingredient for F_{nm} is the exciton density function $\rho(\mathbf{r})$, which is solved numerically.

A. Exciton wave function

It is convenient to use a_B for the length unit, and the exciton binding energy ϵ_B for the energy unit. The Hamiltonian $H_{\rm r}$ in (2) is rotationally invariant around the z axis parallel to B. Therefore the z component of the angular momentum m is a good quantum number with respect to the operator L_z. Since only the ground state with $m = 0$ has a finite oscillator strength proportional to $\rho(0)$, we focus on the eigenfunction with $m = 0$ and drop the second term in (2),

$$H_{\rm r} = -\nabla^2 - 2/r + \frac{\gamma^2}{4} r^2 \sin^2\theta \ , \tag{31}$$

where θ is the polar angle, $\gamma = \hbar\omega_c/2\epsilon_B$, and $\omega_c = eB/\mu c$. This Hamiltonian has been studied by many authors in the past. We solve for the eigenvalues and the eigenfunctions of $H_{\rm r}$ by following the method of Cabib, Fabri, and Fiorio[8] (CFF) closely. A general outline of the method is summarized below, since our new method, presented here, deviates from the variational method of CFF at the last stage.

We transform

$$r = \frac{\alpha\xi}{1-\xi} \ , \tag{32}$$

where α ($=1$ for our numerical analysis presented at the end of this section) is a constant for adjusting the length scale and $0 \le \xi \le 1$. This transform allows us to use a fine grading for small values of r and a coarse grading for large values. The eigenfunction is then expanded in spherical harmonics $Y_{l,0}(\theta,\phi)$,

$$\psi = \sum_l{}' \frac{u_l(\xi)}{\xi} Y_{l,0}(\theta,\phi) \ , \tag{33}$$

where l is summed over zero and even integers (indicated by the prime on $\sum$) up to $l_{\max}$. Only the even angular-momentum states are coupled to the hydrogenic ground state by the last term in (31), which yields nonvanishing matrix elements only for $l' = l$ and $l' = l \pm 2$. The expression in (33) is then inserted in (1) and the $Y_{l,0}$ component is projected out through a dot product.

The resulting second-order differential equation of $u_l(\xi)$ in ξ is converted to a five-point difference equation by evenly dividing $0 \le \xi \le 1$ into small intervals of $\eta = 1/n_{\max} \ll 1$ with $\xi_n = n\eta$ ($n = 1,2,\ldots,n_{\max}$).[8,12] We

find that a sufficient accuracy is achieved with $l_{\max}=10$ and $n_{\max}=100$ in the range of γ studied. By using the Schrödinger equation, one obtains the analytic continuation at the boundary[8]

$$u^0_{-1}=-u^0_1[1+2\alpha\eta(1+\alpha\eta)]+O(\eta^4) \tag{34a}$$

and

$$u^l_{-1}=-u^l_1+O(\eta^4)\quad (l\neq 0)\ , \tag{34b}$$

where $u^l_n=u_l(\xi_n)$. The quantity u^l_n vanishes at the end points $n=0$ and $n=n_{\max}$. In view of the relationships in (34), the five-point difference equations involve u^l_n's where $n=1,\ldots,n_{\max}-1$.

The difference equation is then in the form of $A[u]=\epsilon[u]$, where $[u]$ is a column vector with elements u^l_n. However, the matrix A is non-Hermitian. The matrix equation can be rewritten in the form of a Schrödinger equation with a Hermitian Hamiltonian ($\tilde{H}$) by transforming

$$v^l_n=u^l_n/(1-\xi_n)^2\ . \tag{35}$$

The final eigenvalue equation is then given by

$$\tilde{H}[v^l_n]=\epsilon_{\rm ex}(B)[v^l_n]\ , \tag{36}$$

where $[v^l_n]$ is a $(n_{\max}-1)(l_{\max}+1)$-dimensional column vector. In (36), the matrix elements $\langle l,n|\tilde{H}|l',n'\rangle$ are given by

$$\tilde{H}^{l,l'}_{n,n'}=w^{(n)}_{l,l'}\delta_{n,n'}\quad (l\neq l')\ . \tag{37a}$$

Other nonvanishing matrix elements diagonal in the angular-momentum quantum number (i.e., $l'=l$) are

$$\tilde{H}^{l,l}_{n,n+1}=\tilde{H}^{l,l}_{n+1,n}=-\frac{4}{3\eta^2\alpha^2}\mu_{n,n+1}\ , \tag{37b}$$

$$\tilde{H}^{l,l}_{n,n+2}=\tilde{H}^{l,l}_{n+2,n}=\frac{1}{12\eta^2\alpha^2}\mu_{n,n+2}\ , \tag{37c}$$

$$\tilde{H}^{0,0}_{1,1}=\frac{29(1-\xi_1)^4}{12\eta^2\alpha^2}-\frac{(1-\xi_1)^4}{6\eta\alpha}(1+\eta\alpha)-\frac{2}{r_1}+w^{(1)}_{0,0}\ , \tag{37d}$$

$$\tilde{H}^{l,l}_{1,1}=\frac{29(1-\xi_1)^4}{12\eta^2\alpha^2}+\frac{l(l+1)}{r_1^2}-\frac{2}{r_1}+w^{(1)}_{l,l}\quad (l\neq 0)\ , \tag{37e}$$

and

$$\tilde{H}^{l,l}_{n,n}=\frac{5(1-\xi_n)^4}{2\eta^2\alpha^2}+\frac{l(l+1)}{r_n^2}-\frac{2}{r_n}+w^{(n)}_{l,l}\quad (n\geq 2)\ , \tag{37f}$$

where $r_n=\alpha\xi_n/(1-\xi_n)$, $\mu_{n,m}=(1-\xi_n)^2(1-\xi_m)^2$,

$$w^{(n)}_{l,l}=\tfrac{1}{6}\gamma^2r_n^2\left[1-\frac{l(l+1)}{(2l-1)(2l+3)}\right]\ , \tag{38a}$$

and

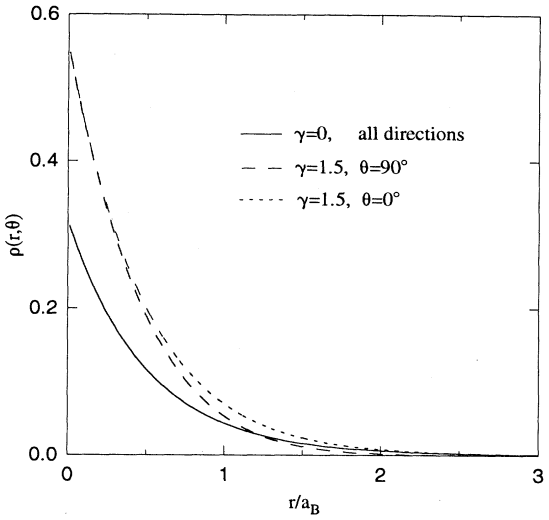

FIG. 1. Exciton probability density function as a function of the radial distance parallel and the polar angle.

$$w^{(n)}_{l,l'}=w^{(n)}_{l',l}=-\frac{\gamma^2r_n^2\delta_{l',l+2}(l+1)(l+2)}{4[(2l+1)(2l+5)]^{1/2}(2l+3)}$$
$$(l'\neq l)\ . \tag{38b}$$

The Hamiltonian defined by Eqs. (36) and (37) is diagonalized on a Cray-YMP computer using a 594×594 matrix (corresponding to $n_{\max}=100$ and $l_{\max}=10$). The ground-state energies coincide with those obtained by Cabib, Fabri, and Fiorio (CFF) to three to four significant digits for $\gamma\leq 5$. The accuracy can be improved by increasing $n_{\max}$ and $l_{\max}$. The normalized density function $\rho(\mathbf{r})$ so obtained is displayed in Fig. 1 at zero field and at $\gamma=1.5$. At zero field, the density decays exponentially at large r, while it decays much faster in a Gaussian form at $\gamma=1.5$. Also, it is clearly seen that the wave function is squeezed in a plane perpendicular to the magnetic field (long-dashed curve) while this effect is much smaller in the parallel direction (short-dashed curve). In order to relate γ to the actual field, we use $\gamma=(a_B/l)^2$, where l is the classical magnetic length. For $In_{0.48}Ga_{0.52}P$ lattice matched to GaAs, we use $\kappa=11.6$ and $\mu=0.075$,[13] obtaining $a_B=81$ Å, $\epsilon_B=7.7$ meV, and $\gamma=0.10B$, where B is in units of tesla. Therefore $\gamma=1.5$ in Fig. 1 corresponds to 15.0 T for $In_{0.48}Ga_{0.52}P/GaAs$.

B. Overlap parameters F_{nm} and $\tilde{F}_{nm}$

The numerical evaluation of the overlap functions in (14) can be simplified if the axial symmetry is utilized in the $\mathbf{k}$ space. Carrying out the Fourier transform for $\rho_{\mathbf{k}}$ in the polar coordinate, we find

$$\rho_{\mathbf{k}}=\frac{2\pi}{k}\sum_l{}'(2l+1)i^lg_l(\mathbf{k})P_l(\cos\theta_{\mathbf{k}})\ , \tag{39a}$$

where

$$g_l(\mathbf{k})=\int\int\rho(\mathbf{r})P_l(\cos\theta)f_l(kr)r\,dr\,\sin\theta\,d\theta\ . \tag{39b}$$

In (39a), $\theta_{\mathbf{k}}$ is the polar angle in $\mathbf{k}$ space, $P_l(z)$ is the

Legendre function, and $f_l(x)$ is related to the Bessel function of a half-odd-integer order $J_{l+1/2}(x)$: $f_l(x)=(\pi x/2)^{1/2}J_{l+1/2}(x)$. Equation (39a) yields a simple result for F_{1m},

$$F_{1m}=\frac{1}{\pi}a_B^3\int\Phi_{\mathbf{k}}^m g_0(\mathbf{k})k\,dk\ , \tag{40}$$

which yields for a Gaussian wave function (i.e., $\Phi_{\mathbf{k}}=\exp[-(kR_0)^2/4]$)

$$F_{1m}=\frac{2a_B^3}{m(\pi m)^{1/2}R_0^3}\times\int\int\rho(\mathbf{r})\exp\left[-\frac{1}{m}\left[\frac{r}{R_0}\right]^2\right]r^2dr\sin\theta\,d\theta\ . \tag{41}$$

We also find in general

$$F_{22}=2a_B^3\int\Phi_{\mathbf{k}}^2\sum_l{}'(2l+1)g_l(\mathbf{k})^2dk\ . \tag{42}$$

Note that the right-hand side of (42) reduces to F_{20} [cf. Eq. (15b)] in the limit $\Phi_{\mathbf{k}}=1$. The overlap parameters $\tilde{F}_{1m}(x)$ and $\tilde{F}_{22}(x)$ are obtained from (41) and (42) by replacing R_0 with xR_0.

Since the function $\tilde{F}_{nm}(x)$ can be obtained from F_{nm}, we consider only F_{nm} in the following qualitative discussion. The field dependences of F_{12} and F_{22} are calculated from Eqs. (41) and (42) and are displayed in Fig. 2 for $R_a/a_B=0$ and $R_0/a_B=1$. They agree with the analytical results $F_{12}=1/\pi$ and $F_{22}=1/8\pi$ for $R_0=0$ and $\gamma=0$. As discussed in the Introduction, the quantities F_{nm} and therefore the field-dependent part of the linewidths [cf. Eqs. (13), (29), and (30)] depend sensitively on the localization length R_0. This effect is clearly seen in Fig. 3, where the R_0 dependences of F_{nm} are plotted at zero field and at $\gamma=1.6$. In the limit $R_0\gg a_B$, however, it should be noted that the linewidth is not given by (29) or (30) but by (18a) with ϵ_0 given by (25) and is independent of the magnetic field, when the localization is induced by the alloy disorder. The overlap factors F_{12} and F_{22} are essentially inversely proportional to the exciton volume $\Omega_{\rm ex}$ for

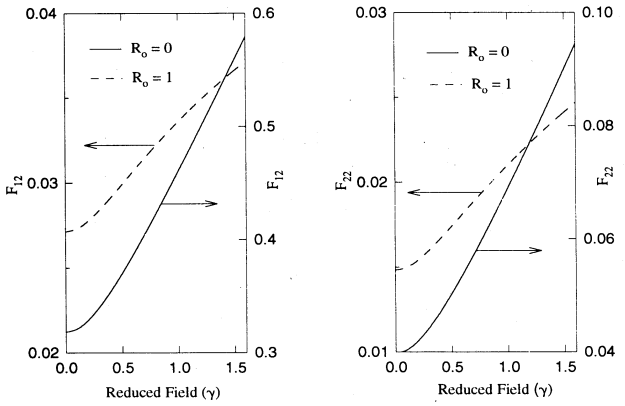

FIG. 2. Overlap parameters F_{12} and F_{22} as a function of the reduced field for $R_0=0$ and 1 (in units of a_B).

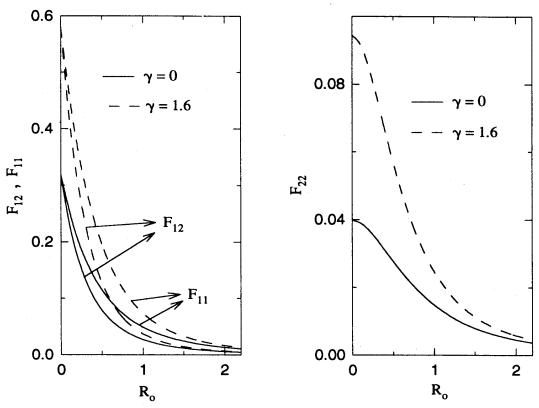

FIG. 3. Overlap parameters F_{nm} as a function of the localization length R_0 (in units of a_B) for zero field and for $\gamma=1.6$. The function $\tilde{F}_{nm}(x)$ is obtained from F_{nm} by the replacement $R_0\rightarrow xR_0$.

$R_0=0$. At high fields, we have $\Omega_{\rm ex}\propto l^2l_z$ where $l\propto B^{-1/2}$ is the classical magnetic length and l_z is the exciton size in the direction of the field. Because l_z is insensitive to the magnetic field,[15] the overlap factors are expected to become nearly linear in B (i.e., γ) for $R_0=0$ in the high-field limit as seen in Fig. 2.

IV. INHOMOGENEOUS LINEWIDTH AND LINE SHAPE

In this section we apply the present theoretical results to recent magnetoluminescence data from disordered $In_{0.48}Ga_{0.52}P$ which show a strong field dependence for the linewidth.[6] Based on the analysis of the FWHM and the line shape presented below, we conclude that the field-dependent linewidth of the cited data[6] arises from the exciton localization at pinning centers.

A. Exciton localization due to pinning centers

In this case, the (normalized) density of states of the exciton energy and therefore the photoluminescence line shape is Gaussian

$$G(\epsilon)=\frac{1}{(2\pi\sigma^2)^{1/2}}\exp\left[-\frac{\epsilon^2}{2\sigma^2}\right]\ , \tag{43}$$

where the mean-square fluctuation energy is given from (13), (8b), and (9) by

$$\sigma^2=\sigma_g^2[\eta_h^3\alpha^2\tilde{F}_{22}(\eta_h)+\eta_e^3(1-\alpha)^2\tilde{F}_{22}(\eta_e)+2\eta_h^3\alpha(1-\alpha)\tilde{F}_{12}(\eta_h)]\ , \tag{44a}$$

with the following limiting behaviors:

$$\sigma^2=\sigma_g^2[\eta_h^3\alpha^2\tilde{F}_{22}(\eta_h)+(1-\alpha)^2(a_B/\sqrt{2\pi}R_0)^3+2\eta_h^3\alpha(1-\alpha)\tilde{F}_{12}(\eta_h)],\quad R_0/a_B\gg m_e/M \tag{44b}$$

and

$$\sigma^2=\sigma_g^2[\eta_h^3\alpha^2F_{20}+\eta_e^3(1-\alpha)^2F_{20} +2\eta_h^3\alpha(1-\alpha)F_{10}(\eta_h)], \quad R_0/a_B \ll m_e/M \ . \tag{44c}$$

In (44), σ_g^2 is given by

$$\sigma_g^2=(dE_g/dx)^2x(1-x)(\Delta V/a_B^3) \ .$$

The quantity α is defined by $dE_e/dx=\alpha dE_g/dx$ and $dE_h/dx=(1-\alpha)dE_g/dx$. The result in (44a) follows from (11) without any approximation except for the factor $\tilde{F}_{12}$ which is accurate in the limit $m_e \ll m_h$. The Gaussian line shape is in approximate agreement with the data.[6] Because F_{12} is much larger than F_{22} (see Fig. 2), the last term of (44a) is as important as the first term therein unless α is very close to unity.

The first, second, and third term in (44) represents, respectively, the contribution from the spatial fluctuations of the conduction, valence, and combined local conduction- and valence-band-edge potential as discussed in the Introduction. In particular, it is transparent that the second term in (44b) describes the mean-square valence-band-edge fluctuation over the volume (αR_0^3) inside the center-of-mass wave function. In order to emphasize the physical meaning of this term (which is a consequence of treating the relative and the center-of-mass coordinates on an equal footing), we consider an extreme case of very small localization length and extremely heavy-hole mass: $R_0=a$ and $R_0/a_B \gg m_e/M$, where a is the lattice constant. In this case, the contribution of the second term to σ^2 in (44a) is of the order $\langle E_h^2 \rangle$. This can be understood in the following way: a hole is localized on a lattice site with an electron bound to it through the Coulomb potential. Because the Bohr radius is much larger than the lattice constant, the mean-square fluctuation of the exciton energy is basically determined by the site-to-site fluctuation of the hole energy $E_h(\mathbf{r}_h)$ and is of the order of $\langle E_h^2 \rangle$.

In Fig. 4 we display the FWHM $\Delta\epsilon_{\rm FWHM}=2.355\sigma$ obtained from (43) and (44) for $dE_g/dx=1.15$ eV.[14] In view of the uncertainty in the parameters $(R_0/a_B,\alpha)$ as well as the wide scatter of the data, we plot the FWHM for three different sets of the parameters $(R_0/a_B,\alpha)$, namely (0, 0.96) in the solid curve, (0.22, 0.89) in the long-dashed curve, and finally (0.34, 0.78) in the short-dashed curve and compare them with the data (open circles) from $In_{0.48}Ga_{0.52}P$.[6] Equation (44a) is employed for the long- and short-dashed curves in Fig. 4 and Eq. (44c) for the solid curve. For these plots, R_0/a_B is not large enough for the limiting expression in Eq. (44b) to be valid. For the long-dashed curve, for example, the first, second, and third term in (44a) yields, respectively, 39%, 20%, and 41% of the contribution to σ^2 at zero field and 46%, 16%, and 38% at 15 T. The fitting is sensitive to the choice of the parameters. It is seen in Fig. 4 that smaller localization radius yields a steeper slope for the curve. The results of LB correspond to the first term of (44c) with $\alpha=1$ (i.e., $dE_h/dx=0$) and with a somewhat different coefficient.

The second derivatives of the functions F_{22} and F_{12} in (44) as a function of the field are positive, vanishing at high fields. The FWHM behaves as $\Delta\epsilon_{\rm FWHM} \propto \sqrt{B}$ at high fields according to the scaling argument presented at the end of Sec. III. As a result, the FWHM has a positive curvature at low fields and a negative curvature at high fields. The inflection points occur near 12 T for the theoretical curves in Fig. 4. A preliminary evidence of this behavior was observed recently by Jones *et al.* in a high-field experiment in $In_{0.48}Ga_{0.52}P$.[16]

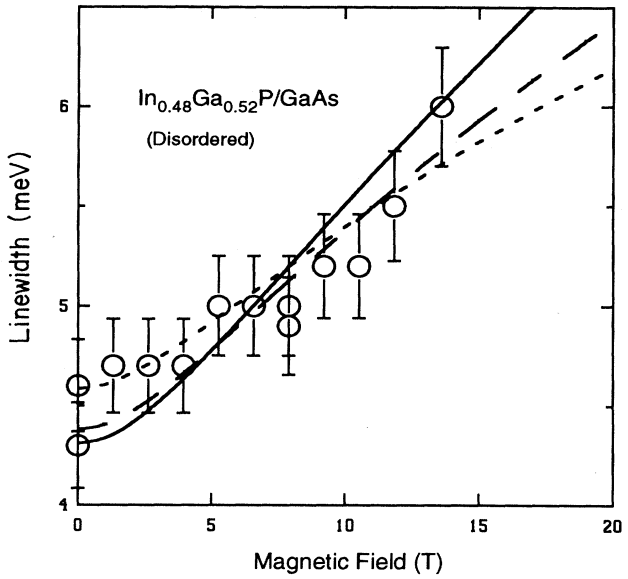

FIG. 4. FWHM as a function of the magnetic field calculated from (44c) (solid curve) and from (44a) (dashed curves) using the defect pinning model. The parameters used for the fitting are given in the text. The data are from Ref. 6.

B. Exciton localization due to alloy disorder

When the exciton localization is caused by alloy disorder, the line shape is given by

$$f(\epsilon)=\int_0^\infty g(x)G(\epsilon-x)dx \ , \tag{45}$$

where the parameters ϵ_0 and σ^2 defined in (28) and (29) are to be used for $g(x)$ and $G(\epsilon)$, respectively. In Fig. 5 we display the normalized line-shape function for $\epsilon_0=0.14$ meV and $\sigma_e=4.2$ meV at zero field (solid curve) and for $B=10$ T (dashed curve). Since the energy x in $g(x)$ in (45) is measured from the bottom of the conduction band into the gap, higher energies in Fig. 5 correspond to lower photon energies. The line shape is asymmetric with a long tail toward the low-photon-energy side, in disagreement with the apparent Gaussian line shape of the data.[6] The FWHM determined from the line shape is plotted in Fig. 6 as a function of the magnetic field (solid curve). The quantity ϵ_0 determines the major part of the zero-field line width and σ_e the field-induced increase of the linewidth. The quantity F_{22} in (29) is approximated by F_{20} in order to estimate the upper bound

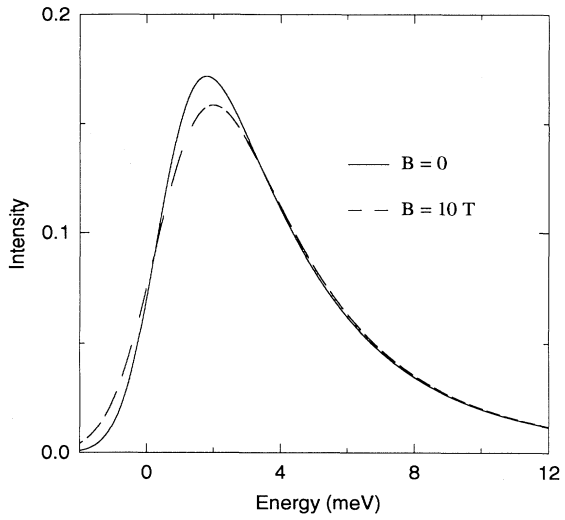

FIG. 5. Normalized line shapes resulting from alloy disorder [Eq. (45)] at 0 and 10 T. Higher energy here corresponds to lower photon energy.

for the FWHM, although the exciton energy does not quite satisfy the condition in (26): $\epsilon \gg \epsilon_c$. The value $\sigma_e = 4.2$ meV corresponds to $dE_e/dx = 0.9$ eV, while $\epsilon_0 = 0.14$ meV requires $dE_h/dx = 0.87$ eV. Recent data[13] indicate that the valence-band offset between GaP and InP is about 0.36 meV. We expect dE_h/dx to be less than 0.36 meV for $In_{0.48}Ga_{0.52}P$ because of the bowing effect. Since the quantity ϵ_0 is proportional to $(dE_h/(dx)^4$, a more realistic ϵ_0 is too small to explain the data. For small ϵ_0, the linewidth is independent of the field as discussed earlier. To summarize, the line shape is

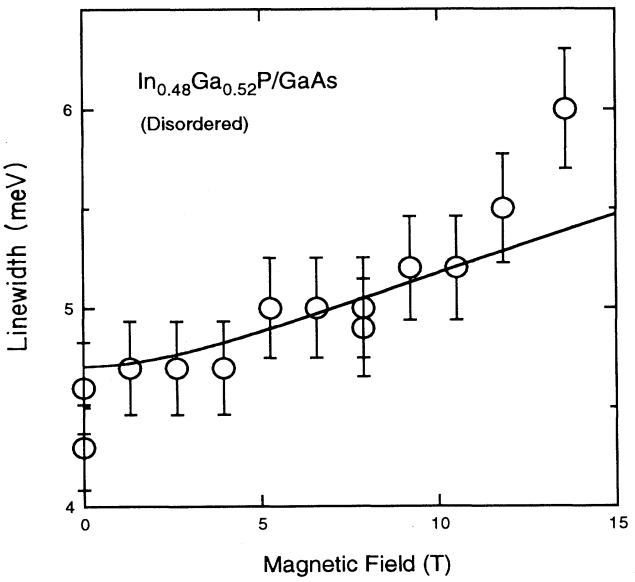

FIG. 6. The FWHM determined from the line shape in Fig. 5, plotted as a function of the magnetic field.

asymmetric with a long tail on the low-photon-energy side and the calculated linewidth is much narrower than the experimental data in the presence of alloy disorder only. More suitable systems for observing this kind of field-dependent linewidth with an asymmetric line shape in the absence of pinning centers are the II-VI alloys because of their large band offsets and exciton binding energies.

In the preceding analysis, we have ignored the possibility of domain fluctuations in the sample. Domain fluctuations of the energy are independent of the field and are Gaussian. The contribution from domain fluctuations can be included by adding the mean-square domain fluctuation to σ^2 in (44) as well as in (29). We have also assumed that cations are distributed at random microscopically and assumed one cation per ΔV. It is possible or even probable that cations may cluster during the growth process, yielding a larger effective volume for ΔV and thus a larger linewidth; a large cluster size will decrease the number of the independent uncorrelated cells inside the exciton volume and thereby increase the fluctuation.

V. SUMMARY

We have developed a theory for the field-dependent inhomogeneous photoluminescence linewidth and the line shape of excitons due to alloy disorder in undoped semiconductor alloys. The linewidth was found to depend not only on the exciton wave function for the electron-hole relative motion but also sensitively on the localization length R_0 of the center-of-mass wave function. The linewidth as well as the strength of its field dependence is larger for smaller R_0. The central results are given by Eqs. (11), (13), (27), (29), (44), and (45) and differ from previous results.[1–5]

The linewidths arise from the fluctuations of the conduction- and valence-band edges in the region with significant amplitude of the total exciton wave function. The wave function for the relative motion was calculated numerically by reducing the Schrödinger equation to a difference equation at arbitrary fields, while the center-of-mass wave function was treated phenomenologically.

Two types of exciton localization have been considered: pinning by defect centers and localization by alloy disorder. The former leads to a symmetric Gaussian line shape and a strongly field-dependent FWHM in good agreement with the recent data from $In_{0.48}Ga_{0.52}P$. The latter yields an asymmetric line shape and smaller linewidths in disagreement with the $In_{0.48}Ga_{0.52}P$ data. The effects of clustering of the cations and the domain fluctuation on the linewidth were discussed.

ACKNOWLEDGMENTS

The author thanks Dr. E. D. Jones for a critical reading of the manuscript, for many valuable discussions on the subject, and for making the data available prior to publication. He is also grateful to Dr. D. M. Follstaedt for a helpful discussion on the TEM results of the sample cited in Ref. 6. This work was supported by the Division of Materials Science, Office of Basic Energy Science, U.S. DOE under Contract No. DEAC04-76DP00789.

[1]O. Goede, L. John, and D. Hennig, Phys. Status Solidi B **89**, K183 (1978).
[2]E. F. Schubert, E. O. Göbel, Y. Horikoshi, K. Ploog, and H. J. Queisser, Phys. Rev. B **30**, 814 (1984).
[3]J. Singh and K. K. Bajaj, Appl. Phys. Lett. **48**, 1077 (1986) and references therein.
[4]S. M. Lee and K. K. Bajaj, Appl. Phys. Lett. **60**, 853 (1992).
[5]R. A. Mena, G. D. Sanders, and K. K. Bajaj, J. Appl. Phys. **70**, 1866 (1991).
[6]E. D. Jones, R. P. Schneider, Jr., S. M. Lee, and K.K. Bajaj, Phys. Rev. B **46**, 7225 (1992).
[7]E. D. Jones (private communication).
[8]D. Cabib, E. Fabri, and G. Fiorio, Nuovo Cimento B **10**, 185 (1972).
[9]W. Lamb, Phys. Rev. **85**, 259 (1952).
[10]S. D. Baranovskii and A. L. Éfros, Fiz. Tekh. Poluprovodn. **12**, 2233 (1978) [Sov. Phys. Semicond. **12**, 1428 (1978)].
[11]V. Sa-yakanit, Phys. Rev. B **19**, 2266 (1979).
[12]S. E. Koonin and D. C. Meredith, *Computational Physics, Fortran Version* (Addison-Wesley, New York, 1990), p. 6.
[13]M. P. C. M. Krijn, Semicond. Sci. Technol. **6**, 27 (1991).
[14]*Landolt-Börnstein Series III*, edited by O. Madelung (Springer, New York, 1987), Vol. 22a, p. 141.
[15]H. Hasegawa and R. E. Howard, J. Phys. Chem. Solids **21**, 179 (1961).
[16]E. D. Jones *et al.* (unpublished).